Bioelectrochemistry 144 (2022) 108000

Contents lists available at ScienceDirect

Bioelectrochemistry

journal homepage: www.elsevier.com/locate/bioelechem

Ultrasensitive label-free electrochemical biosensor for detecting linear microcystin-LR using degrading enzyme MlrB as recognition element

Yanfang Li [a], Sisi Si [a], Feiyu Huang [c], Jia Wei [c], Shengyi Dong [d], Fei Yang [b,*], Huimin Li [a,*], Song Liu [a,*]

[a] Institute of Chemical Biology and Nanomedicine (ICBN), State Key Laboratory of Chemo/Biosensing and Chemometrics, College of Chemistry and Chemical Engineering, Hunan University, Changsha 410082, PR China
[b] Hunan Province Key Laboratory of Typical Environmental Pollution and Health Hazards, School of Public Health, University of South China, Hengyang 421001, PR China
[c] Hunan Provincial Key Laboratory of Clinical Epidemiology, Xiangya School of Public Health, Central South University, Changsha 410078, PR China
[d] College of Chemistry and Chemical Engineering, Hunan University, Changsha, Hunan 410082, PR China

ARTICLE INFO

Article history:
Received 24 August 2021
Received in revised form 22 October 2021
Accepted 11 November 2021
Available online 16 November 2021

Keywords:
Linear microcystin-LR
MlrB
Electrochemical biosensor
Multi-walled carbon nanotube
Square wave voltammetry

ABSTRACT

A label-free electrochemical biosensor was firstly constructed to detect linear microcystin-LR (L-MC-LR) with high sensitivity. Degradation enzyme MlrB was used as recognition element for specific recognition of L-MC-LR. The electrode was modified with –COOH functionalized multi-walled carbon nanotube to increase the specific surface area and improve the conductivity, which was then applied to immobilize MlrB. The electrochemical signal was changed with the reaction between MlrB and L-MC-LR, which was recorded by using square wave voltammetry. The electrochemical biosensor showed superior sensitivity, with a dynamic range of 1 pg/mL to 100 ng/mL and a detection limit of 0.127 pg/mL. Moreover, the fabricated electrochemical biosensor exhibited excellent specificity toward L-MC-LR in real water samples. The concentrations of spiked L-MC-LR were 0.100, 5.00, 50.0 ng/mL, and the recovery rates were 95.0–104% with relative standard deviation (RSD) of 0.900–2.30% and 74.0–93.0% with RSD of 2.30–3.50% in lake water and tap water, respectively. Furthermore, the selectivity, reproducibility, and stability demonstrated the potential of degradation enzymes as recognition element in detection of cyanotoxins.
© 2021 Elsevier B.V. All rights reserved.

1. Introduction

Cyanobacterial blooms caused by eutrophication have become global environmental concerns [1]. Large numbers of freshwater lakes are infested with cyanobacteria, which pollute water sources by releasing microcystins (MCs) [2]. Microcystin-LR (MC-LR) is a variant of cyanotoxins with maximum toxicity, and its common degradation intermediate linear microcystin-LR (L-MC-LR) is also highly toxic [3]. The existence of L-MC-LR in water is a direct and widespread threat to human health. Detection of L-MC-LR in water is of great significance not only for water quality monitoring, but also for exploring the biodegradation mechanism of MC-LR during water treatment [4].

Currently, several methods have been reported for the detection of MCs, including enzyme-linked immunosorbent assay [5], thin layer chromatography [6], protein phosphatase inhibition assays [7,8], liquid chromatography-mass spectrometry [9–11], and nuclear magnetic resonance [12]. However, these methods have been limited by various shortcomings, such as unfavorable specificity and sensitivity, time consuming, high cost, the requirement of complicated sample pretreatment and experienced operators [13,14]. The electrochemical biosensor has been a potential method for overcoming these shortcomings, presenting the advantages of high sensitivity, fast response, good selectivity, instrument integration and miniaturization, and on-line continuous monitoring, compatible with complex matrix [15,16]. It is suitable for field analysis.

For improving the selectivity and specificity of electrochemical biosensors, the recognition elements have been constructed to achieve specific detection. Some studies have been performed on the electrochemical detection of MCs. Zhang's group developed an ultra-sensitive electrochemical immunosensor for the specific determination of MCs in real water samples, with antibodies as recognition elements [17]. Under the optimal conditions, the detection limit of the prepared immunosensor was as low as 0.1 ng/L. Another highly sensitive and selective sensor has been reported for the MCs detection, employing unlabeled DNA aptamer as the recognition element. The detection limit was 1.9 pM [18]. Besides of antibody and aptamer, molecularly imprinted polymer (MIP) has been constructed as another kind of recognition element.

* Corresponding authors.
E-mail addresses: phfyang@csu.edu.cn (F. Yang), huiminli@hnu.edu.cn (H. Li), liusong@hnu.edu.cn (S. Liu).

https://doi.org/10.1016/j.bioelechem.2021.108000
1567-5394/© 2021 Elsevier B.V. All rights reserved.

Xu's group integrated MIP of MCs to prepare sensors, providing a new method for monitoring the pollutants in water [19]. However, strong acid or base is required during MIP preparation, leading to the deactivation of template biomolecules. Moreover, the samples with structural change cannot be recognized in MIP, leading to impaired detection sensitivity and accuracy [20]. In short, the exploration of new recognition elements has been crucial and significant.

Recently, several MCs degrading bacteria have been investigated, in which the MCs degradation enzymes exhibited good specificity for MCs. Jones et al. isolated an MCs degrading bacterium ACM-3962 from natural water for the first time, which exhibited a high degradation rate for MC-LR [21]. Further study investigated the degradation pathway of MC-LR by degrading bacterium *Sphingopyxis* sp. ACM-3962 [3]. At least three enzymes (MlrA, MlrB and MlrC) were involved in the degradation of MC-LR. In a previous report, a strain was found to completely degrade MC-LR [22]. In the study on MC-LR degradation pathway, MlrA broke the cyclic heptapeptides of MC-LR and degraded them into L-MC-LR. Then, under the action of MlrB enzyme, the L-MC-LR would be hydrolyzed into tetrapeptides. Finally, MlrC enzyme decomposed the tetrapeptides into small molecular peptides. Yang's group specified the role of linearized-microcystinase in the bacterial utilization of MC-LR and provided a powerful evidence on the roles of enzymes in MC biodegradation [23]. Considering the affinity between enzyme and substrate, we speculated these enzymes can act as recognition receptors for specific recognition of MCs.

Previous methods have used antigen, antibody, aptamer or MIP as biological receptors. In this work, degrading enzyme MlrB was innovatively applied as a recognition element that could specifically bind with L-MC-LR. Multi-walled carbon nanotubes (MWCNTs) have been significant for constructing electrochemical sensors, because of its diversified surface chemistry, superior electrical activity and miniaturization for in-situ detection [24–26]. Modification of the electrode with –COOH functionalized MWCNT (MWCNT-COOH) can not only increase the specific surface area of the electrode, but also facilitate the immobilization of MlrB via functional groups on MWCNT-COOH. The electrochemical properties of the electrode surface will be changed after the binding of MlrB with L-MC-LR, thus it can be used to construct the electrochemical biosensor. Square Wave Voltammetry (SWV) was applied as the signal output mode for effectively reducing the background current and improving detection efficiency. The detection performance of this electrochemical biosensor has been evaluated, and it was also tested in the real water samples.

2. Experimental section

2.1. Chemicals and reagents

MWCNT (>95%, 30 ~ 50 nm in diameter, 10 ~ 30 μm in length) was purchased from XFNANO Materials Tech Co., Ltd. (Nanjing, China). Bovine serum albumin (BSA, AR), chitosan (CS, 99%, AR) were purchased from J&K Scientific Ltd. (Beijing, China). 1-pyrenebutanoic acid N-hydroxysuccinimide ester (PBASE, AR) was purchased from Sigma-Aldrich (USA). Potassium ferricyanide ($K_3Fe(CN)_6$, ≥ 99.5%, AR), potassium ferrocyanide trihydrate trihydrate ($K_4Fe(CN)_6{\cdot}3H_2O$, ≥ 99.5%, AR), potassium chloride (KCl, ≥ 99.5%, AR) were purchased from Sinopharm Chemical Reagent Co., Ltd. (Shanghai, China). The MlrA and MlrB enzymes were obtained by recombinant *E. coli* overexpressing the *mlrA* and *mlrB* genes of *Sphingopyxis* sp. YF1, and purified by glutathione S-transferase-Accept nickel column as previous reported [22]. All aqueous solutions were prepared with ultrapure water with a resistivity of 18.2 MΩ·cm.

2.2. Apparatus

All electrochemical measurements were performed using a CHI 660E electrochemical workstation (Shanghai Chenhua Instrument Co., Ltd, China), with glass carbon electrodes (GCE, 3 mm) as working electrode, platinum wire as count electrode, and $Hg/HgCl_2$ as the reference electrode. All the electrochemical measurements were performed in air at room temperature and atmosphere pressure. Scanning electron microscopy (SEM) images were captured by Hitachi S4800 operated at 20 kV. Transmission electron microscopy (TEM) was carried out by using JEM-2100Plus instrument at an acceleration voltage of 200 kV. The X-ray photoelectron spectroscopy (XPS) measurements were conducted on ESCALAB 250Xi to investigate the chemical composition and valence states of element. Raman spectrum was performed with a 532 nm excitation laser and a 100× objective (WITec, Germany). Fourier transform infrared spectrum (FT-IR) was obtained from an IRSpirit spectrometer (Shimadzu, Japan).

2.3. Synthesis of MWCNT-COOH

The MWCNT-COOH was prepared[13] (Scheme 1A). 20 mg of MWCNT was mixed with 20 mL of mixture (HNO_3:H_2SO_4 = 1: 3). After evenly stirred, the mixture was ultrasonically treated at 80 ℃ for 4 h. After centrifuging (10,000 rpm, 5 min) and washing until pH was neutral, the product was vacuum dried at 80 ℃ for 12 h. After that, the MWCNT-COOH was re-dispersed in 0.25% CS to prepare the solution with a series of concentration. Finally, the as-prepared MWCNT-COOH was stored at room temperature for further use.

2.4. Construction of the biosensor

The construction of the biosensor was demonstrated (Scheme 1B). Before using the GCE was polished with 1.0 μm and 0.05 μm alumina slurry in turn to obtain a mirror-like surface. After washing and drying, 5 μL of as-prepared MWCNT-COOH suspension was dropped on the cleaned bare GCE and air-dried at room temperature to form a film. 7 μL of PBASE was dropped on the surface of the electrode and incubated at room temperature for 1 h. Then 7 μL of MlrB was immobilized onto the electrode at 4 ℃ overnight. Unbound MlrB was removed with PBS. 10 μL of 0.5% BSA was added and incubated for 1 h at 4 ℃ to block the non-specific adsorption. After that, the sensor electrode was washed with PBS thoroughly. The counterpart electrode without MlrB modification was prepared with the same method as control.

2.5. Electrochemical measurement of L-MC-LR by the biosensor

The prepared BSA/MlrB/MWCNT-COOH/GCE electrode was incubated with 5 μL of L-MC-LR solution with different concentrations (1 pg/mL to 100 ng/mL) for 30 min at room temperature, then the modified electrode was washed thoroughly with PBS to wash off the nonspecific adsorption. Cyclic voltammetry (CV), SWV, and electrochemical impedance spectroscopy (EIS) were performed in 2.5 mM $[Fe(CN)_6]^{3-/4-}$ solution containing 0.1 M KCl. CV and SWV have been obtained at −0.1 to 0.5 V. The frequency range was between 1 Hz and 100,000 Hz, with a signal amplitude of 5 mV for EIS. The reference electrode was saturated calomel electrode (0.241 V) throughout the measurement.

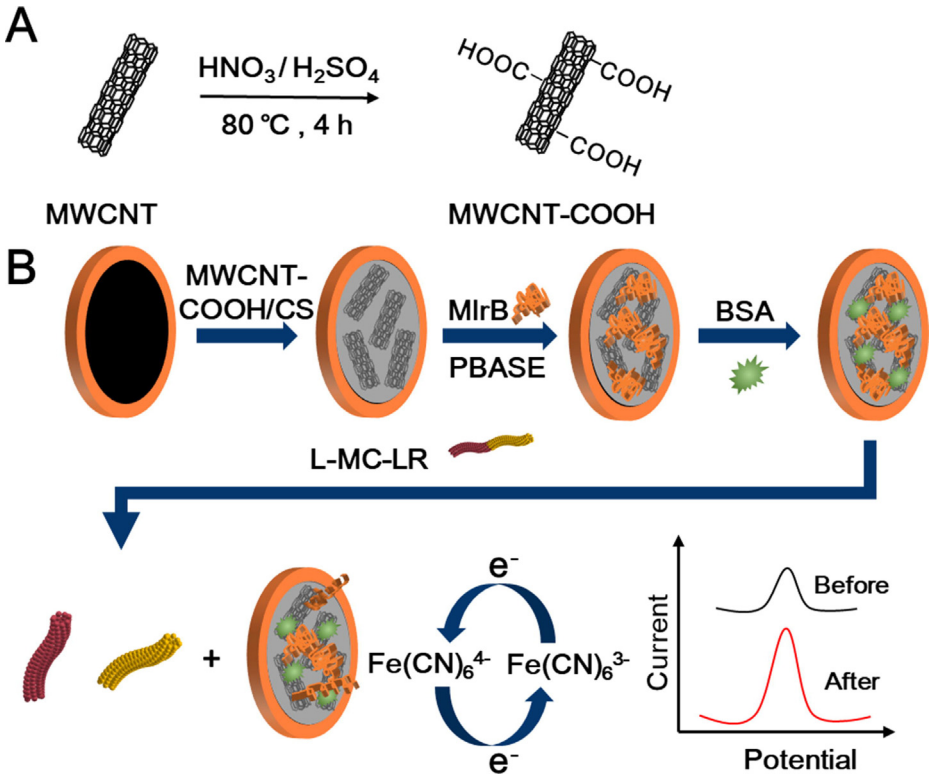

Scheme 1. The electrochemical biosensor. (A) The modification of MWCNT. (B) The fabrication and working of electrochemical biosensor.

3. Results and discussions

3.1. Characterization of the MWCNTs

The MWCNTs turned to be hydrophilic after oxidation. After standing for two weeks, the MWCNTs before oxidation were deposited at the bottom, while the MWCNTs after oxidation were uniformly dispersed in the aqueous solution (Fig. 1A). The MWCNT-COOH was characterized with SEM and TEM (Fig. 1B and C). The surface of MWCNT-COOH was smooth without the trace of fracture, suggesting that the morphological structure of carbon tubes was not damaged during functionalization. The MWCNT-COOH modified with enzyme MlrB was also characterized with SEM (Fig. S1). The characteristic peaks of MWCNT-COOH were observed in the FT-IR spectra, including C-O stretching, C=O stretching and O-H stretching peaks (Fig. S2). All these peaks prove the existence of MWCNT-COOH.

The Raman spectra of MWCNT and MWCNT-COOH were presented (Fig. 1D). Two distinct peaks at 1340 cm^{-1} and 1568 cm^{-1} referred to the D and G bands of the MWCNTs. The D band corresponded to the disordered structure of the tube wall. The G band indicated the graphitic nature of the carbon nanotubes, resulted from the stretching bond of sp^2 carbon atoms from both ring and chain types. After functionalization, the intensity ratio of D band and G band (I_D/I_G) was changed from 0.45 to 0.94, proving the successful modification of the MWCNTs. Higher I_D/I_G suggested more defects. After acidifying, two characteristic peaks of carbon tubes were shifted to 1348 cm^{-1} and 1579 cm^{-1}. Meanwhile, the D band appeared as a shoulder to the G band at 1616 cm^{-1}. All these changes can be attributed to the formation of oxygen-containing functional groups on the surface of MWCNT-COOH.

The XPS survey spectra (Fig. 1E) confirmed the presence of C and O elements on MWCNT-COOH. In the deconvolution of C1s (Fig. 1F), the characteristic peak at 284.7 eV was belong to C=C/C-C as the carbon skeleton of MWCNT-COOH. Besides, the characteristic peaks observed at 285.5 eV, 286.6 eV, and 288.9 eV were attributable to C-OH, C=O, and COOH, respectively, indicating the generation of hydroxyl and carboxyl groups on the surface of MWCNTs. As for the deconvolution of O1s (Fig. 1G), the peaks at 531.9 eV, 533.5 eV, and 536.2 eV were representative of typical C=O, C-O, and O=C-O groups. The results of C1s and O1s in XPS were consistent with those of in FT-IR spectra, verifying the successful oxidation of MWCNTs.

3.2. Electrochemical characterization of the biosensor

The biosensor was assembled layer by layer and the change of electrochemical signal was recorded with CV (Fig. 2A) and EIS (Fig. 2B). The bare GCE show a pair of symmetric redox peaks, indicating smooth and clean electrode surface. After acidifying, the redox current of MWCNT-COOH was dramatically increased. This might be attributed to the good conductivity of MWCNT-COOH, which improved the electron transfer rate of $[Fe(CN)_6]^{3-/4-}$. After modification with MlrB, the current was remarkably decreased. This was resulted from the poor conductivity of MlrB as biomacromolecule, as well as the steric hindrance, both of which prevented the transfer of $[Fe(CN)_6]^{3-/4-}$ to the electrode surface and reduced the rate of electron transfer. The current was further reduced after blocking with BSA. The redox current was increased after adding a certain amount of L-MC-LR solution. In this process, the configuration of MlrB was changed to degrade L-MC-LR specifically. Thus, the charge on the surface of the electrode was also varied, which affected the electron transfer rate of $[Fe(CN)_6]^{3-/4-}$.

EIS is a technique to study the relation between alternating current impedance and frequency of electrochemical systems under the constant current polarization and equilibrium potential. The impedance spectrum consisted of a semicircle part in the high-frequency region determined by the charge transfer process, and

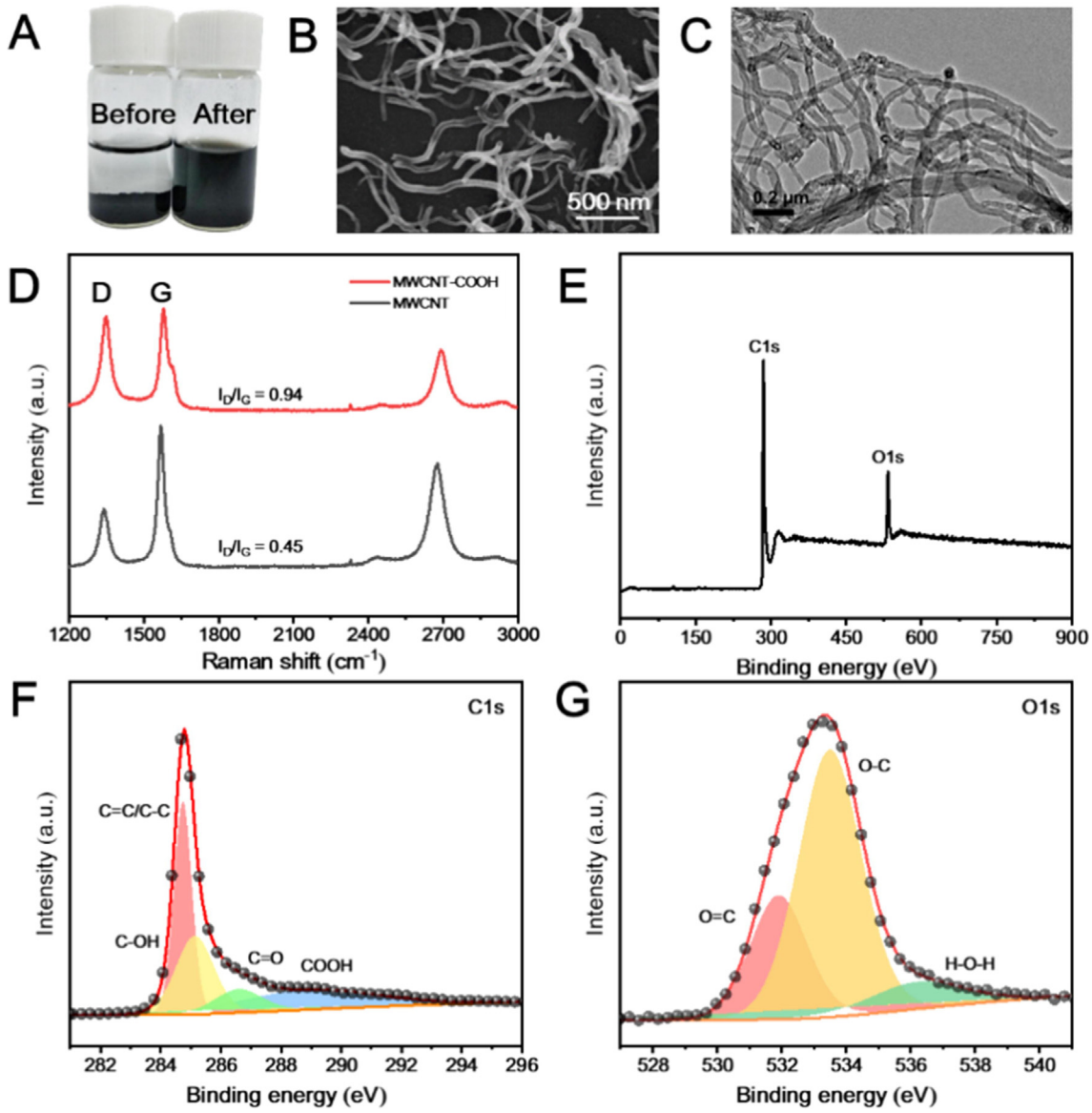

Fig. 1. (A) MWCNT solution before and after oxidation and leaving for 2 weeks. (B) SEM and (C) TEM images of MWCNT-COOH. (D) Raman spectra of MWCNT and MWCNT-COOH. (E) XPS survey spectra of MWCNT-COOH. (F) The deconvolution of C 1s and (G) O 1s.

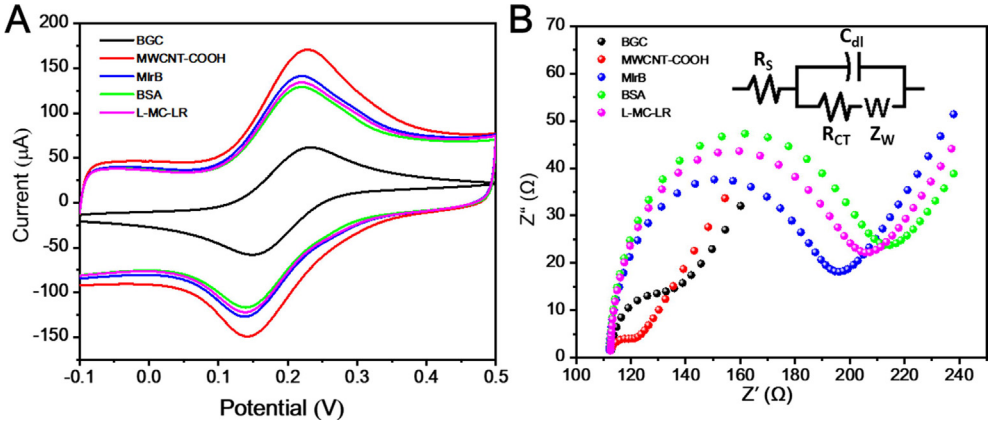

Fig. 2. (A) CV and (B) EIS for bare GCE, MWCNT-COOH/GCE, MIrB/MWCNT-COOH/GCE, BSA/MIrB/MWCNT-COOH/GCE, and L-MC-LR/BSA/MIrB/MWCNT-COOH/GCE obtained in 2.5 mM $[Fe(CN)_6]^{3-/4-}$ solution at open circuit potential. Note: R_s, C_{dl} represent the solution ohmic resistance and double-layer capacitance between the reference electrode and the working electrode, respectively. R_{ct} indicates electron-transfer resistance of the $[Fe(CN)_6]^{3-/4-}$ at the interface of the electrode. Z_w is the diffusional impedance from the electrolyte to the electrode surface.

a straight part in the low-frequency region controlled by the diffusion process (Fig. 2B). The impedance value of each modification stage was calculated by fitting the data through the equivalent circuit diagram (internal illustration in Fig. 2B). The electron-transfer resistance of the $[Fe(CN)_6]^{3-/4-}$ at the interface of the electrode was indicated by R_{ct}, which was 19.43, 8.52, 74.50, 90.06, and 83.00 Ω for GCE, MWCNT-COOH/GCE, MlrB/MWCNT-COOH/GCE, BSA/MlrB/MWCNT-COOH/GCE, and L-MC-LR/BSA/MlrB/MWCNT-COOH/GCE (Fig. 2B). It was worth noting that the variation trend of EIS was consistent with the variation of the CV spectra. Due to the good electrical properties of MWCNT, R_{ct} was the smallest in the MWCNT-COOH/GCE electrode. The CV and EIS results confirmed the good performance of electrochemical biosensor. To prove that the signal was resulted from the specific interaction between MlrB and L-MC-LR, control experiments were performed. No significant signal change can be observed on the counterpart electrode without coating MlrB (Fig. S3).

The relationship between the sweep rate and the peak current was obtained by CV scanning on the same electrode. The sweep rate was changed from 40 mV/s to 200 mV/s in 2.5 mM $[Fe(CN)_6]^{3-/4-}$ solution containing 0.1 M KCl (Fig. 3). It can be clearly seen that the peak currents of both anode and cathode were increased with the accelerated sweep speed. As shown in inset of Fig. 3, the relationship between the redox peak currents and the square root of scan rates was linear, indicating that the electrochemical process of the redox molecules on the biosensor was diffusion-dependent.

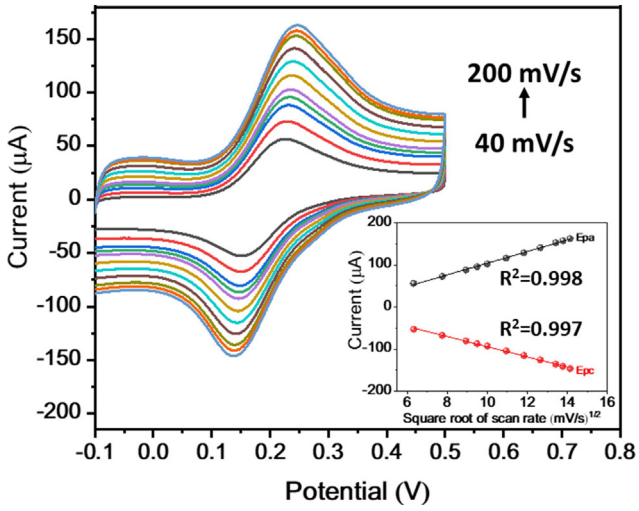

Fig. 3. CV spectra of the electrochemical biosensor with different scan rates (40 mV/s ~ 200 mV/s), which are performed in 2.5 mM $[Fe(CN)_6]^{3-/4-}$ solution containing 0.1 M KCl. Inset: the linear fitting of redox peak currents and the square root of scan rates.

3.3. Optimization of the detection conditions

The performance of biosensors can be affected by several factors, such as the concentration of MWCNT-COOH, the concentration of MlrB, incubation time of L-MC-LR, and pH value of buffer. The effects of MWCNT-COOH concentration on CV peak current were presented (Fig. S4). The peak current represented the reaction rate of $[Fe(CN)_6]^{3-/4-}$ on the electron surface. When the MWCNT-COOH concentration was increased from 1 to 3 mg/mL, the peak current was rapidly increased. It was not significantly increased when the concentration was further increased from 3 to 5 mg/mL. The 3 mg/mL was thus determined as the optimal MWCNT-COOH concentration in terms of electron conductivity and system reversibility.

The number of recognition receptors immobilized on the electrode also affected the sensitivity of sensor. The effects of MlrB concentration on peak current change rate ($\Delta I/I_0$: $\Delta I = I_0 - I$, I_0: current before MlrB modification, I: current after MlrB modification) were shown (Fig. 4A). The $\Delta I/I_0$ aggrandized sharply when MlrB concentration was increased from 0 to 300 μg/mL. It was resulted from the negative charge and steric hindrance of MlrB, thus limiting the electron transfer of $[Fe(CN)_6]^{3-/4-}$ on the electrode surface. The $\Delta I/I_0$ was not significantly changed when the MlrB concentration was further increased because of the saturation and equilibrium. Hence, 300 μg/mL was chose as optimal MlrB concentration.

The influence of incubation time of L-MC-LR on the detection performance of BSA/MlrB/MWCNT-COOH/GCE was further investigated (Fig. 4B). The electrochemical signal was obviously increased when the incubation time was increased from 10 to 30 min, then it remained with prolonged incubation time. The reaction may achieve an equilibrium. Thus, the incubation time of L-MC-LR was set as 30 min.

The pH value of buffer had a significant effect on the detection performance of electrochemical biosensors. The pH value affected not only the modification efficiency of MlrB on electrodes but also its further catalytic activity. The relationship of SWV peak current change (ΔI) and the pH value (6.0 to 8.5) was investigated (Fig. 4C), with the concentration of L-MC-LR fixed at 1 ng/mL. The ΔI was increased sharply with the increase of pH value, reached the maximum value at pH = 7.4, and then diminished slightly with further increased pH value. The pH value of 7.4 was applied as the optimal pH value of buffer.

3.4. Electrochemical detection of L-MC-LR

The performance of electrochemical detection of L-MC-LR was evaluated under the optimum conditions. Different concentrations of L-MC-LR (1 pg/mL–100 ng/mL) were added on the developed electrochemical biosensors for recording the SWV response (Fig. 5A). The peak current was enhanced successively with the

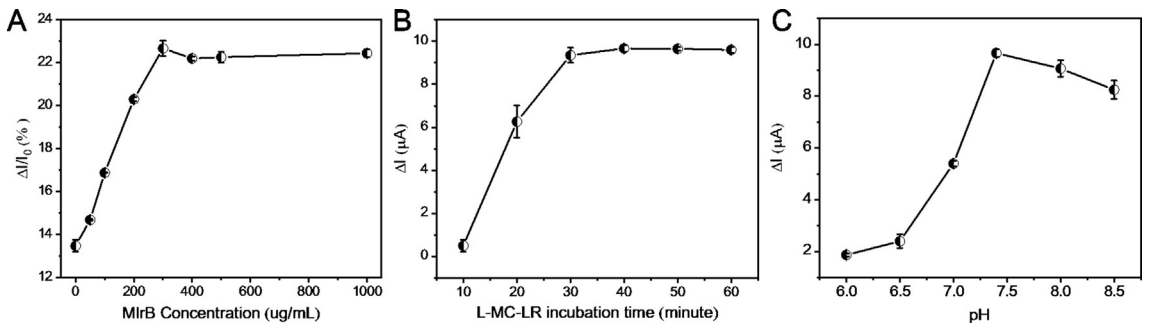

Fig. 4. Optimization of the detection conditions. The peak current change rate with increased concentration of MlrB (A), L-MC-LR incubation time (B) and pH value of buffer (C).

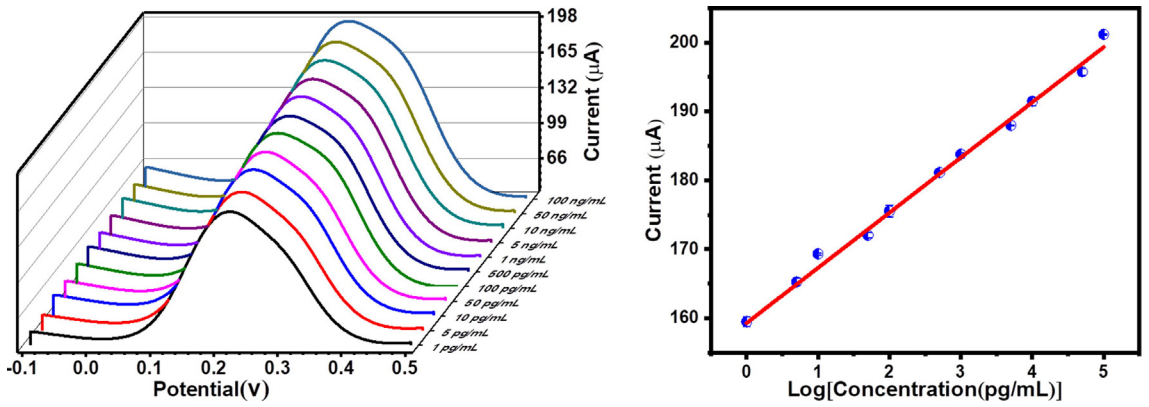

Fig. 5. Electrochemical detection of L-MC-LR. (A) SWV response of electrochemical biosensor towards different concentrations of L-MC-LR (1 pg/mL ~ 100 ng/mL). (B) Linear fitting plot between the current and the logarithmic concentration of L-MC-LR. The equation relating to the curve is I (μA) = 159.3 + 8.01 log[C(pg/mL)] (R^2 = 0.980).

increased L-MC-LR concentration. There was a good linearity between the current and the logarithm of L-MC-LR concentration (ranged from 1 pg/mL to 100 ng/mL), with R^2 of 0.980 (Fig. 5B). The correlation equation was fitted as: I (μA) = 159.3 + 8.01 log [C(pg/mL)], and the detection limit was calculated as 0.127 pg/mL (S/N = 3). There was no report on the content of L-MC-LR in drinking water, considering the known maximum acceptable concentration of MC-LR in water was 1 μg/L, this biosensor was promising in meeting the requirements of L-MC-LR detection.

The detection of MCs has triggered extensive research, as shown in Table 1. Depending on the biological receptors, different types of biosensors have been studied extensively, but there are still some limitations. At present, there are still few detection methods for L-MC-LR, so our method provides a new strategy.

3.5. Selectivity, reproducibility, and stability of the biosensor

The selectivity of the constructed electrochemical biosensor for L-MC-LR was evaluated by incubating the biosensor with some potential interferents, including PBS (1 ×), Ca^{2+} (10 pM), Cu^{2+} (10 pM), MC-LR (10 ng/mL), and microcystin-RR (MC-RR, 10 ng/mL). As displayed in Fig. 6A, only L-MC-LR (1 ng/mL) caused a significant current response, while no other interferents induced obvious signal changes. These results demonstrated that the prepared biosensors presented good selectivity to L-MC-LR detection.

The repeatability of the biosensor was further investigated. Five independent electrodes were used to detect L-MC-LR (1 ng/mL) under optimal conditions. By comparing SWV peak currents of every electrode, the obtained relative standard deviation (RSD) was 1.40%, suggesting a good repeatability (Fig. 6B).

Table 1
Detection of MCs using various types of biosensors.

Bioreceptor	Lower limit (μg/L)	Upper limit (μg/L)	LOD (μg/L)	Reference
MC-LR antigen	0.0025	5.0	0.0016	[27]
MC-LR Abs	0.050	20	0.050	[28]
MC-LR aptamer	0.010	50	0.0020	[29]
MIP of MCs	1.0	1.0×10^3	0.0093	[19]
enzyme MlrB of L-MC-LR	1.0×10^{-3}	1.0×10^2	1.3×10^{-4}	

Abbreviations: Ab, antibody; LOD, limit of detection (the minimal amount of toxin whose presence or absence can be detected).

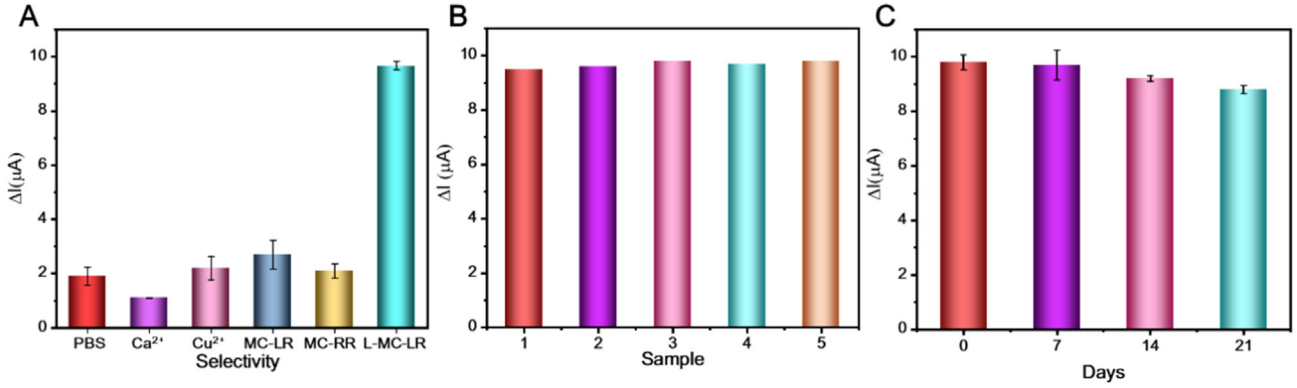

Fig. 6. (A) Selectivity of the electrochemical biosensor to L-MC-LR (1 ng/mL) compared with PBS (1×), Ca^{2+} (10 pM), Cu^{2+} (10 pM), MC-LR (10 ng/mL), and MC-RR (10 ng/mL). (B) Reproducibility of the electrochemical biosensor was examined by detecting L-MC-LR (1 ng/mL) with five independent biosensors under the same conditions. (C) Stability of the electrochemical biosensor was examined by detecting L-MC-LR (1 ng/mL) with different storage time (0–21 days).

The stability of the biosensor was studied by comparing the SWV peak currents before and after storing at 4 ℃ for 21 days. The enzyme activity remained 93.9% and 89.8% after 14 and 21 days, indicating the good stability of the biosensor (Fig. 6C).

3.6. Application to L-MC-LR analysis in real water samples

The feasibility of applying the prepared biosensor for L-MC-LR detection was verified in real water samples. Then, the standard addition method was applied. The real water samples were lake water and tap water collected in Hunan University. Based on the above experiment, the sensitivity of the biosensor was evaluated in real water samples. In lake water samples, there was a good linearity between the current and the logarithm of L-MC-LR concentration. The equation relating to the curve is I (μA) = 333.5 9 + 2.53 log[C(pg/mL)] (R^2 = 0.969), and the detection limit was calculated as 2.11 pg/mL (S/N = 3) (Fig. S5). The concentrations of spiked L-MC-LR were 0.100, 5.00, 50.0 ng/mL, and the recovery rates were 95.0–104% with relative standard deviation (RSD) of 0.900–2.30% and 74.0–93.0% with RSD of 2.30–3.50% in lake water and tap water, respectively (Table S1). The low recovery rate in tap water may be due to the effects of chlorine in tap water on L-MC-LR, which affected the specific recognition of MlrB towards L-MC-LR. The detection results indicated that the developed biosensor was feasible to monitor L-MC-LR in real water.

4. Conclusion

In this work, a label-free electrochemical sensor based on degrading enzyme MlrB was successfully constructed to detect L-MC-LR. MlrB has been applied as a recognition element in the electrochemical sensor for the first time. Furthermore, the functionalized MWCNT was applied as substrate for loading MlrB. SWV was involved as a detection method for improving the detection sensitivity and saving the detection time. Under optimal conditions, the enzyme-based electrochemical sensor exhibited a wide dynamic range for the L-MC-LR detection. The proposed method exhibited good specificity, stability, and reproducibility, with acceptable recovery rate in real water samples. This label-free electrochemical sensor provides a new strategy for the detection of harmful cyanotoxins in water, which is of great significance for environmental monitoring and degradation mechanism study.

Declaration of Competing Interest

The authors declare that they have no known competing financial interests or personal relationships that could have appeared to influence the work reported in this paper.

Acknowledgements

The work gratefully acknowledges financial support from the National Natural Science Foundation of China (No. 21975067), Hunan Province Excellent Youth Fund (2020JJ3053), National Natural Science Foundation of China (81773393), and Fundamental Research Funds for the Central Universities from Hunan University.

Appendix A. Supplementary material

Supplementary data to this article can be found online at https://doi.org/10.1016/j.bioelechem.2021.108000.

References

[1] J. Huisman, G.A. Codd, H.W. Paerl, B.W. Ibelings, J.M.H. Verspagen, P.M. Visser, Cyanobacterial blooms, Nat. Rev. Microbiol. 16 (8) (2018) 471–483, https://doi.org/10.1038/s41579-018-0040-1.
[2] X. Zhang, X. Ye, L. Chen, H. Zhao, Q. Shi, Y. Xiao, L. Ma, X. Hou, Y. Chen, F. Yang, Functional role of bloom-forming cyanobacterium Planktothrix in ecologically shaping aquatic environments, Sci. Total Environ. 710 (2020), https://doi.org/10.1016/j.scitotenv.2019.136314 136314.
[3] D.G. Bourne, G.J. Jones, R.L. Blakeley, A. Jones, A.P. Negri, P. Riddles, Enzymatic pathway for the bacterial degradation of the cyanobacterial cyclic peptide toxin microcystin LR, Appl. Environ. Microbiol. 62 (11) (1996) 4086–4094, https://doi.org/10.1128/aem.62.11.4086-4094.1996.
[4] D. Dziga, G. Zielinska, B. Wladyka, O. Bochenska, A. Maksylewicz, W. Strzalka, J. Meriluoto, Characterization of Enzymatic Activity of MlrB and MlrC Proteins Involved in Bacterial Degradation of Cyanotoxins Microcystins, Toxins 8 (3) (2016), 10.3390/toxins8030076.
[5] R. Kurmayer, G. Christiansen, J. Fastner, T. Borner, Abundance of active and inactive microcystin genotypes in populations of the toxic cyanobacterium Planktothrix spp, Environ. Microbiol. 6 (8) (2004) 831–841, https://doi.org/10.1111/emi.2004.6.issue-810.1111/j.1462-2920.2004.00626.x.
[6] I. Meisen, U. Distler, J. Müthing, S. Berkenkamp, K. Dreisewerd, W. Mathys, H. Karch, M. Mormann, Direct Coupling of High-Performance Thin-Layer Chromatography with UV Spectroscopy and IR-MALDI Orthogonal TOF MS for the Analysis of Cyanobacterial Toxins, Anal. Chem. 81 (10) (2009) 3858–3866, https://doi.org/10.1021/ac900217q.
[7] J.E. Noble, P. Ganju, A.E.G. Cass, Fluorescent Peptide Probes for High-Throughput Measurement of Protein Phosphatases, Anal. Chem. 75 (9) (2003) 2042–2047, https://doi.org/10.1021/ac025838e.
[8] D.O. Mountfort, P. Holland, J. Sprosen, Method for detecting classes of microcystins by combination of protein phosphatase inhibition assay and ELISA: comparison with LC-MS, Toxicon 45 (2) (2005) 199–206, https://doi.org/10.1016/j.toxicon.2004.10.008.
[9] J.L. Graham, K.A. Loftin, M.T. Meyer, A.C. Ziegler, Cyanotoxin Mixtures and Taste-and-Odor Compounds in Cyanobacterial Blooms from the Midwestern United States, Environ. Sci. Technol. 44 (19) (2010) 7361–7368, https://doi.org/10.1021/es1008938.
[10] A. Zastepa, F.R. Pick, J.M. Blais, A. Saleem, Analysis of intracellular and extracellular microcystin variants in sediments and pore waters by accelerated solvent extraction and high performance liquid chromatography-tandem mass spectrometry, Anal. Chim. Acta 872 (2015) 26–34, https://doi.org/10.1016/j.aca.2015.02.056.
[11] L. Zhang, X. Ping, Z. Yang, Determination of microcystin-LR in surface water using high-performance liquid chromatography/tandem electrospray ionization mass detector, Talanta 62 (1) (2004) 191–198, https://doi.org/10.1016/j.talanta.2003.07.001.
[12] W. Ma, W. Chen, R. Qiao, C. Liu, C. Yang, Z. Li, D. Xu, C. Peng, Z. Jin, C. Xu, S. Zhu, L. Wang, Rapid and sensitive detection of microcystin by immunosensor based on nuclear magnetic resonance, Biosens. Bioelectron. 25 (1) (2009) 240–243, https://doi.org/10.1016/j.bios.2009.06.020.
[13] Z. He, Y. Cai, Z. Yang, P. Li, H. Lei, W. Liu, Y. Liu, A dual-signal readout enzyme-free immunosensor based on hybridization chain reaction-assisted formation of copper nanoparticles for the detection of microcystin-LR, Biosens. Bioelectron. 126 (2019) 151–159, https://doi.org/10.1016/j.bios.2018.10.033.
[14] P. Pang, X. Teng, M. Chen, Y. Zhang, H. Wang, C. Yang, W. Yang, C.J. Barrow, Ultrasensitive enzyme-free electrochemical immunosensor for microcystin-LR using molybdenum disulfide/gold nanoclusters nanocomposites as platform and Au@Pt core-shell nanoparticles as signal enhancer, Sens. Actuators B Chem. 266 (2018) 400–407, https://doi.org/10.1016/j.snb.2018.03.154.
[15] E. Bakker, Y. Qin, Electrochemical Sensors, Anal. Chem. 78 (12) (2006) 3965–3984, https://doi.org/10.1021/ac060637m.
[16] Z. Wang, H. Guo, R. Gui, H. Jin, J. Xia, F. Zhang, Simultaneous and selective measurement of dopamine and uric acid using glassy carbon electrodes modified with a complex of gold nanoparticles and multiwall carbon nanotubes, Sens. Actuators B Chem. 255 (2018) 2069–2077, https://doi.org/10.1016/j.snb.2017.09.010.
[17] J. Zhang, Z. Xiong, Z. Chen, Ultrasensitive electrochemical microcystin-LR immunosensor using gold nanoparticle functional polypyrrole microsphere catalyzed silver deposition for signal amplification, Sens. Actuators B Chem. 246 (2017) 623–630, https://doi.org/10.1016/j.snb.2017.02.134.
[18] S. Eissa, A. Ng, M. Siaj, M. Zourob, Label-Free Voltammetric Aptasensor for the Sensitive Detection of Microcystin-LR Using Graphene-Modified Electrodes, Anal. Chem. 86 (15) (2014) 7551–7557, https://doi.org/10.1021/ac501335k.
[19] Z. Qi, R. Lu, S. Wang, C. Xiang, C. Xie, M. Zheng, X. Tian, X. Xu, Selective fluorometric determination of microcystin-LR using a segment template molecularly imprinted by polymer-capped carbon quantum dots, Microchem. J. 161 (2021), https://doi.org/10.1016/j.microc.2020.105798 105798.
[20] Z. Wu, D. He, B. Cui, Z. Jin, Ultrasensitive detection of microcystin-LR with gold immunochromatographic assay assisted by a molecular imprinting technique, Food Chem. 283 (2019) 517–521, https://doi.org/10.1016/j.foodchem.2019.01.064.
[21] G.J. Jones, D.G. Bourne, R.L. Blakeley, H. Doelle, Degradation of the cyanobacterial hepatotoxin microcystin by aquatic bacteria, NAT TOXINS 2 (4) (1994) 228–235, https://doi.org/10.1002/nt.2620020412.

[22] F. Yang, F. Huang, H. Feng, J. Wei, I.Y. Massey, G. Liang, F. Zhang, L. Yin, S. Kacew, X. Zhang, Y. Pu, A complete route for biodegradation of potentially carcinogenic cyanotoxin microcystin-LR in a novel indigenous bacterium, Water Res. 174 (2020), https://doi.org/10.1016/j.watres.2020.115638 115638.
[23] J. Wei, F. Huang, H. Feng, I.Y. Massey, T. Clara, D. Long, Y. Cao, J. Luo, F. Yang, Characterization and Mechanism of Linearized-Microcystinase Involved in Bacterial Degradation of Microcystins, Front. Microbiol. 12 (527) (2021), https://doi.org/10.3389/fmicb.2021.646084.
[24] H.R. Jamei, B. Rezaei, A.A. Ensafi, Ultra-sensitive and selective electrochemical biosensor with aptamer recognition surface based on polymer quantum dots and C60/MWCNTs- polyethylenimine nanocomposites for analysis of thrombin protein, Bioelectrochemistry 138 (2021), https://doi.org/10.1016/j.bioelechem.2020.107701 107701.
[25] Y.-H. Wang, Y.-X. Chen, X. Wu, K.-J. Huang, Electrochemical biosensor based on Se-doped MWCNTs-graphene and Y-shaped DNA-aided target-triggered amplification strategy, Colloids Surf. B 172 (2018) 407–413, https://doi.org/10.1016/j.colsurfb.2018.08.064.
[26] Y. Sun, X. He, J. Ji, M. Jia, Z. Wang, X. Sun, A highly selective and sensitive electrochemical CS–MWCNTs/Au-NPs composite DNA biosensor for Staphylococcus aureus gene sequence detection, Talanta 141 (2015) 300–306, https://doi.org/10.1016/j.talanta.2015.03.052.
[27] J. Zhang, Y. Sun, H. Dong, X. Zhang, W. Wang, Z. Chen, An electrochemical non-enzymatic immunosensor for ultrasensitive detection of microcystin-LR using carbon nanofibers as the matrix, Sens. Actuators B Chem. 233 (2016) 624–632, https://doi.org/10.1016/j.snb.2016.04.145.
[28] W. Zhang, C. Han, B. Jia, C. Saint, M. Nadagouda, P. Falaras, L. Sygellou, V. Vogiazi, D.D. Dionysiou, A 3D graphene-based biosensor as an early microcystin-LR screening tool in sources of drinking water supply, Electrochimica Acta 236 (2017) 319–327, https://doi.org/10.1016/j.electacta.2017.03.161.
[29] J. Lv, S. Zhao, S. Wu, Z. Wang, Upconversion nanoparticles grafted molybdenum disulfide nanosheets platform for microcystin-LR sensing, Biosens. Bioelectron. 90 (2017) 203–209, https://doi.org/10.1016/j.bios.2016.09.110.